

**Brazilian Journal of
Chemical Engineering**

**3D compositional reservoir simulation in conjunction with
unstructured grids**

Journal:	<i>Brazilian Journal of Chemical Engineering</i>
Manuscript ID:	BJCE-2015-0011
Manuscript Type:	Original Article
Date Submitted by the Author:	07-Jan-2015
Complete List of Authors:	Araújo, André; Federal Institute of Education, Science and Technology of Ceará, Mechanical Engineering Fernandes, Bruno; Federal University of Ceará, Chemical Engineering Drumond Filho, Edilson; Federal University of Ceará, Chemical Engineering Araujo, Robson; Federal University of Ceará, Chemical Engineering Lima, Ivens; Federal University of Ceará, Chemical Engineering Gonçalves, Alysson; Federal University of Ceará, Chemical Engineering Marcondes, Francisco; Universidade Federal do Ceará, Departamento de Engenharia Metalurgica e de Materiais Sepehrnoori, Kamy; The University of Texas at Austin, Petroleum and Geosystems Engineering
Keyword:	EbFVM, Compositional reservoir simulation, IMPEC approach, Unstructured grids

SCHOLARONE™
Manuscripts

1
2 **3D COMPOSITIONAL RESERVOIR SIMULATION IN CONJUNCTION WITH**
3 **UNSTRUCTURED GRIDS**
4
5
6
7
8
9

10 André Luíz de Souza Araújo
11
12 Federal Institute of Education, Science and Technology of Ceará, Fortaleza, Ceará, Brazil
13
14
15

16 Bruno Ramon Batista Fernandes
17
18 Laboratory of Computational Fluid Dynamics, Federal University of Ceará, Brazil
19
20
21
22

23 Edilson Pimentel Drumond Filho
24
25 Laboratory of Computational Fluid Dynamics, Federal University of Ceará, Brazil
26
27
28
29

30 Robson Melo Araujo
31
32 Laboratory of Computational Fluid Dynamics, Federal University of Ceará, Brazil
33
34
35

36 Ivens da Costa Menezes Lima
37
38 Laboratory of Computational Fluid Dynamics, Federal University of Ceará, Brazil
39
40
41
42

43 Alysson Daniel Ribeiro Gonçalves
44
45 Laboratory of Computational Fluid Dynamics, Federal University of Ceará, Brazil
46
47
48
49

50 Francisco Marcondes*

51 Department of Metallurgy and Materials Science and Engineering, Federal University of
52
53 Ceará, Brazil
54
55
56
57
58
59
60

2

1
2
3 Kamy Sephrnoori
4
5 Center for Petroleum and Geosystems Engineering, The University of Texas at Austin, USA
6
7
8
9
10
11
12
13
14
15
16
17
18
19
20
21
22
23
24
25
26
27
28
29
30
31
32
33
34
35
36
37
38
39
40
41
42
43
44
45
46
47
48
49
50
51
52
53
54
55
56
57
58
59
60

*full corresponding information

① Term used before definition.

3

1
2
3 **Abstract.** In last decade, unstructured grids have been a very important step in the
4 development of petroleum reservoir simulators. In fact, the so-called third generation
5 simulators are based on PEBI unstructured grids. Nevertheless, the use of PEBI grids is not
6 so general when full anisotropic reservoirs are modelled. Another possibility is the use of the
7 Element based Finite Volume Method (EbFVM). This approach has been tested to several
8 reservoir types and in principle has no limitation in application. In this paper, we implement
9 this approach in an in-house simulator called UTCOMP using four element types:
10 hexahedron, tetrahedron, prism, and pyramid. UTCOMP is a compositional,
11 multiphase/multi-component simulator based on an Implicit Pressure Explicit Composition
12 (IMPEC) approach designed to handle several hydrocarbon recovery processes. All
13 properties, except permeability and porosity are evaluated in each grid vertex. In this work,
14 four cases studies were selected to evaluate the implementation, two of them involving
15 irregular geometries. Results are shown in terms of oil and gas rates and saturated gas field.
16
17
18
19
20
21
22
23
24
25
26
27
28
29
30
31
32
33
34
35
36
37
38
39
40
41
42
43
44
45
46
47
48
49
50
51
52
53
54
55
56
57
58
59
60

Keywords: EbFVM, compositional reservoir simulation, IMPEC approach, unstructured grids

1. INTRODUCTION

The proper petroleum reservoir modelling requires the correct evaluation of several important geometric parameters, such as sealing faults, fractures, irregular reservoir shapes, and deviated wells. Although simple to use, conventional Cartesian grids, commonly employed in petroleum reservoir simulation, cannot produce accurate modelling of most of the aforementioned geometry features. The first applications of unstructured grids in petroleum reservoir area were carried by Forsyth 1990 (Fung et al. 1991; Gottardi et al. 1992). The above-mentioned authors conducted a 2D discretization of material balance

equations using linear triangle elements. The approach developed in these works was called Control Volume Finite Element Method (CVFEM). The multicomponent/multiphase approximate equations were obtained from the single phase equations multiplied by phase mobilities. Verma and Aziz (2002) and Edwards (2002) developed the multipoint-flux approach. In this method, all physical properties are stored in each vertex of the grid, including the porosity and the absolute permeability tensor. This method was implemented for triangular and quadrilateral elements. One drawback of this approach is the necessity to solve a local linear system in order to maintain the flux continuity. This issue is raised by the storage of permeability in each vertex of the grid. Using the Element based Finite-Volume Method (EbFVM), as presented in this paper, and storing one permeability tensor, for each element, overcomes this problem. Furthermore, fully heterogeneous and anisotropic reservoirs can also be handled using this approach.

Several studies have been conducted in order to further develop and enhance the CVFEM method. Cordazzo (2004) and Cordazzo et al. (2004) applied the ideas of Raw (1985) and Baliga and Patankar (1983) to simulate water flooding problems. Concerning the final governing equations, this method is very similar to the CVFEM. (The main difference between CVFEM and EbFVM techniques lies in the assumption of multiphase/multi-component flow of the EbFVM approach in order to obtain the approximated equations.) The resulting approach was called Element-based Finite Volume Method (EbFVM), which is a more suitable denomination, since it borrows the flexibility of the finite-element method to discretize the domain, but keeps the conservative idea from the finite-volume method. Later, Paluszny et al. (2007) presented a full tridimensional discretization for hexahedron, tetrahedron, prism, and pyramid elements in conjunction with water flooding problems. Marcondes and Sepehrnoori (2010) and Marcondes et al. (2013) applied the EbFVM to 2D and 3D isothermal, compositional problems in conjunction with a fully implicit approach.

PE
SC

???

Santos et al. (2013) applied the EbFVM to the solution of 3D compositional miscible gas flooding with dispersion, once again associated with the fully implicit approach. These works demonstrated that much more accurate solutions can be obtained with the EbFVM compared to the Cartesian grids. Fernandes et al. (2013) investigated several interpolation functions for the solution of compositional problems for 2D reservoir in conjunction with the EbFVM approach.

This work presents an investigation of the EbFVM method for the solution of isothermal, multicomponent/multiphase flows in 3D reservoirs using four element types: hexahedron, tetrahedron, prism and pyramid in conjunction with an IMPEC (Implicit Pressure Explicit Composition) approach. The porosity and permeability tensor are constant throughout each element. All remaining properties are evaluated at the vertices of each element, defining a cell-vertex approach. The method was implemented in the UTCOMP simulator, developed at the Center of Petroleum and Geosystems Engineering at The University of Texas at Austin for handling several compositional, multiphase/multicomponent recovery processes.

2. GOVERNING EQUATIONS

According to Wang et al. (1997), in order to describe an isothermal, multiphase/multicomponent flow in a porous medium it requires the evaluation of three types of equations: the material balance for all components, the phase equilibrium equations, and the equations for constraining phase saturations and component concentrations.

The material balance equation for each component is given by

$$\frac{1}{V_b} \frac{\partial N_i}{\partial t} - \vec{\nabla} \cdot \sum_{j=1}^{n_p} [\xi_j \lambda_j x_j \bar{k} \cdot \vec{\nabla} \Phi_j] - \frac{q_i}{V_b} = 0 \quad \text{for } i = 1, 2, \dots, n_c \quad (1)$$

where N_i is the number of moles of the i -th component, ξ_j , λ_j , and y_j are respectively, the molar density, the molar mobility, and the molar weight of the j -th phase, x_{ij} is the molar fraction of the i -th component in j -th phase, q_i is the molar rate of the i -th component, V_b is bulk volume, \bar{k} is the absolute permeability tensor, and Φ_j is the potential phase of the j -th phase which is given by

$$\Phi_j = P_j - \gamma_j D + P_{ejr}, \quad \text{is this eqn correct?} \quad [P] = \frac{M}{L^2} \quad [\rho_{ejr}] = \frac{M}{L^2}$$

where P_j is the pressure of the j -th phase, P_{ejr} represents the capillary pressure between phases j and r , and D is the reservoir depth which is positive in the downward direction. In UTCOMP, the oil phase is the reference phase.

Following the material balance, the phase equilibrium calculation must be performed. The phase equilibrium calculations are necessary to determinate the number and composition of all phases, satisfying three conditions. First, the molar-balance equation has to be considered. Next, the chemical potentials for each component must be the same for every phase. The last condition is the minimization of the Gibbs free energy. The first partial derivate for the total Gibbs free energy for the independent variables results in the equality of all component fugacities throughout all phases.

$$f_i^j - f_i^r = 0 \quad (i=1,2,\dots,n_c; j=2,\dots,n_p-1). \quad (3)$$

Notice that the water phase is not included in the phase equilibrium calculations.

The phase composition constraints and the equation for determining the phase amounts for both hydrocarbon phases are respectively, given by

$$\sum_{i=1}^{n_c} x_{ij} - 1 = 0 \quad (j=1,2,\dots,n_p), \quad (4)$$

$$\sum_{i=1}^{n_c} \frac{z_i (K_i - 1)}{1 + v (K_i - 1)} = 0. \quad (5)$$

In Eq. (5), K_i stands for the equilibrium ratio for each component, z_i is the overall molar fraction, and v represents the gas mole fraction in the absence of water.

The last equation to be obtained is the pressure equation. The UTCOMP simulator is based on an IMPEC (Implicit Pressure, Explicit Composition) approach. In this formulation, the pressure is solved implicitly, while the conservations, Eq. (1), are evaluated explicitly. In each grid block, the pressure is obtained from the assumption that the pore volume is completely filled with the total volume of fluid

$$V_t(P, N) = V_p(P), \quad (6)$$

where the pore volume (V_p) is a function only of the pressure, while the total fluid volume (V_t) is a function of pressure and the total number of moles of each component. Differentiating each side of Eq. (6) with respect to their independent variables, the pressure equation (Acs et al. 1985; Chang 1990) is reached as follows:

$$\begin{aligned} & \frac{1}{V_b} \left(V_p^0 c_f - \frac{\partial V_p}{\partial P} \right) \left(\frac{\partial P}{\partial t} \right) - \sum_{i=1}^{n_c+1} \bar{V}_i \vec{\nabla} \cdot \sum_{j=1}^{n_p} \lambda_{ij} \xi_j x_{ij} \bar{k} \cdot \vec{\nabla} P \\ &= \sum_{i=1}^{n_c+1} \bar{V}_i \vec{\nabla} \cdot \sum_{j=1}^{n_p} \lambda_{ij} \xi_j x_{ij} \bar{k} \cdot (\vec{\nabla} P_{cjo} - \gamma_j \vec{\nabla} D) + \frac{1}{V_b} \sum_{i=1}^{n_c+1} \bar{V}_i q_i, \end{aligned} \quad (7)$$

where \bar{V}_i represents the derivative of total fluid volume related to N_i .

3. APPROXIMATE EQUATIONS

The EbFVM method is characterized by the division of each element into sub-elements according to the number of vertices. Conservation equations, Eqs. (1) and (7), are integrated over each sub-element. After the division of the elements into sub-elements, we call them sub-control volumes. The material balance is established for every sub-control volume, and

then, the control volume balance equation is built by adding the contributions of every sub-control volume that shares the same vertex.

Each element type has a certain sub-control volume division based on the number of vertices. Figure 1 shows the division for each of the four elements investigated in this work, according to the number of vertices. From Figure 1, it is possible to infer that each sub-control volume for hexahedron, prism, and tetrahedron elements is composed of three integration surfaces. The exception is the pyramid element whose sub-control volumes associated with the base have three integration surfaces, in which two integration surfaces are triangular and one is quadrilateral; the sub-control volume associated with the apex has four integration surfaces, and all of them are quadrilaterals. In Fig. 1, the numbers that reside inside a circle refer to the integration surface and the others refer to the vertices.

Figure 1

Integrating Eq. (1) in time and over each sub-control volume, followed by the application of the Gauss theorem for advective term, we obtain:

$$\int_{V_b} \frac{\partial N_i}{\partial t} dV dt - \int_{A_J} \sum_{j=1}^{n_p} \xi_j x_j \lambda_j \bar{k} \cdot \vec{\nabla} \Phi_j \cdot d\bar{A} dt - \int_{V_b} \frac{q_i}{V} dV dt = 0 ; i=1, 2, \dots, n_{ch} \quad (8)$$

In order to evaluate volume, area and gradient in Eq. (8), it is necessary to define the shape functions for each element type. The shape functions for hexahedron, tetrahedron, prism, and pyramid elements are, respectively defined, as follows:

$$\begin{aligned} N_1(s, t, p) &= \frac{(1+s)(1-t)(1+p)}{8} ; N_2(s, t, p) = \frac{(1+s)(1-t)(1-p)}{8} \\ N_3(s, t, p) &= \frac{(1-s)(1-t)(1-p)}{8} ; N_4(s, t, p) = \frac{(1-s)(1-t)(1+p)}{8} \\ N_5(s, t, p) &= \frac{(1+s)(1+t)(1+p)}{8} ; N_6(s, t, p) = \frac{(1+s)(1+t)(1-p)}{8} \\ N_7(s, t, p) &= \frac{(1-s)(1+t)(1-p)}{8} ; N_8(s, t, p) = \frac{(1-s)(1+t)(1+p)}{8}, \end{aligned} \quad (9)$$

1
2
3 $N_1(s, t, p) = 1 - s - t - p ; \quad N_2(s, t, p) = s$
4 $N_3(s, t, p) = t ; \quad N_4(s, t, p) = p,$

5
6
7 $N_1(s, t, p) = (1 - s - t)(1 - p) ; \quad N_2(s, t, p) = s(1 - p)$
8 $N_3(s, t, p) = t(1 - p) ; \quad N_4(s, t, p) = p(1 - s - t)$
9
10 $N_5(s, t, p) = sp ; \quad N_6(s, t, p) = tp,$

11
12 $N_1(s, t, p) = \frac{1}{4}[(1 - s)(1 - t) - p + stp / (1 - p)]$
13
14 $N_2(s, t, p) = \frac{1}{4}[(1 + s)(1 - t) - p - stp / (1 - p)]$
15
16 $N_3(s, t, p) = \frac{1}{4}[(1 + s)(1 + t) - p - stp / (1 - p)]$
17
18 $N_4(s, t, p) = \frac{1}{4}[(1 - s)(1 + t) - p - stp / (1 - p)]$
19
20
21 $N_5(s, t, p) = p .$

22
23
24
25 In the shape function equations presented above s , t , and p are the coordinates in a local
26 reference frame, defined in each element. This local frame allows all elements to be treated
27 equally, regardless how distorted an element is in the global x , y , and z system. Since we
28 employ the shape functions to evaluate any physical property or geometry position inside
29 each element, these elements are called isoparametric elements (Hughes 1987).

30
31
32 $x(s, t, p) = \sum_{i=1}^{N_v} N_i x_i ; \quad y(s, t, p) = \sum_{i=1}^{N_v} N_i y_i ;$
33
34 $z(s, t, p) = \sum_{i=1}^{N_v} N_i z_i ; \quad \Phi_j(s, t, p) = \sum_{i=1}^{N_v} N_i \Phi_{ji} .$

35
36
37 In Eq. (13), N_v and N_i denote the number of vertices and the shape functions of each
38 element, respectively. From Eq. (13), the gradient of phase potential can be written as
39

40
41 $\frac{\partial \Phi_j}{\partial x} = \sum_{i=1}^{N_v} \frac{\partial N_i}{\partial x} \Phi_{ji} ; \quad \frac{\partial \Phi_j}{\partial y} = \sum_{i=1}^{N_v} \frac{\partial N_i}{\partial y} \Phi_{ji} ; \quad \frac{\partial \Phi_j}{\partial z} = \sum_{i=1}^{N_v} \frac{\partial N_i}{\partial z} \Phi_{ji}$

42
43
44 The shape functions derivatives required to compute the gradients in Eq. (14) are given
45 by

$$\begin{aligned}
 \frac{\partial N_i}{\partial x} &= \frac{1}{\det(J_i)} \left(\frac{\partial y}{\partial t} \frac{\partial z}{\partial p} - \frac{\partial y}{\partial p} \frac{\partial z}{\partial t} \right) \frac{\partial N_i}{\partial s} - \frac{1}{\det(J_i)} \left(\frac{\partial y}{\partial s} \frac{\partial z}{\partial p} - \frac{\partial y}{\partial p} \frac{\partial z}{\partial s} \right) \frac{\partial N_i}{\partial t} \\
 &\quad + \frac{1}{\det(J_i)} \left(\frac{\partial y}{\partial s} \frac{\partial z}{\partial t} - \frac{\partial y}{\partial t} \frac{\partial z}{\partial s} \right) \frac{\partial N_i}{\partial p} \\
 \frac{\partial N_i}{\partial y} &= -\frac{1}{\det(J_i)} \left(\frac{\partial x}{\partial t} \frac{\partial z}{\partial p} - \frac{\partial x}{\partial p} \frac{\partial z}{\partial t} \right) \frac{\partial N_i}{\partial s} + \frac{1}{\det(J_i)} \left(\frac{\partial x}{\partial s} \frac{\partial z}{\partial p} - \frac{\partial x}{\partial p} \frac{\partial z}{\partial s} \right) \frac{\partial N_i}{\partial t} \\
 &\quad - \frac{1}{\det(J_i)} \left(\frac{\partial x}{\partial s} \frac{\partial z}{\partial t} - \frac{\partial x}{\partial t} \frac{\partial z}{\partial s} \right) \frac{\partial N_i}{\partial p} \\
 \frac{\partial N_i}{\partial z} &= \frac{1}{\det(J_i)} \left(\frac{\partial x}{\partial t} \frac{\partial y}{\partial p} - \frac{\partial x}{\partial p} \frac{\partial y}{\partial t} \right) \frac{\partial N_i}{\partial s} - \frac{1}{\det(J_i)} \left(\frac{\partial x}{\partial s} \frac{\partial y}{\partial p} - \frac{\partial x}{\partial p} \frac{\partial y}{\partial s} \right) \frac{\partial N_i}{\partial t} \\
 &\quad + \frac{1}{\det(J_i)} \left(\frac{\partial x}{\partial s} \frac{\partial y}{\partial t} - \frac{\partial x}{\partial t} \frac{\partial y}{\partial s} \right) \frac{\partial N_i}{\partial p},
 \end{aligned} \tag{15}$$

where $\det(J_i)$ is the Jacobian of the transformation and is given for all sub-control volumes by

$$\det(J_i) = \frac{\partial x}{\partial s} \left(\frac{\partial y}{\partial t} \frac{\partial z}{\partial p} - \frac{\partial y}{\partial p} \frac{\partial z}{\partial t} \right) - \frac{\partial x}{\partial t} \left(\frac{\partial y}{\partial s} \frac{\partial z}{\partial p} - \frac{\partial y}{\partial p} \frac{\partial z}{\partial s} \right) + \frac{\partial x}{\partial p} \left(\frac{\partial y}{\partial s} \frac{\partial z}{\partial t} - \frac{\partial y}{\partial t} \frac{\partial z}{\partial s} \right) \tag{16}$$

The sub-control volumes for the hexahedron, tetrahedron, prism, and pyramid elements are given, respectively, by Eqs. (17) through (20), and the area for quadrilateral integration surfaces is given by Eq. (21).

$$V_{sv,i} = \det(J_i), \tag{17}$$

$$V_{sv,i} = \det(J_i)/6, \tag{18}$$

$$V_{sv,i} = \det(J_i)/12, \tag{19}$$

$$V_{sv,i} = \begin{cases} 2 \det(J_i)/9 & \text{for } i=1, \dots, 4 \text{ (base)} \\ 4 \det(J_i)/9 & \text{for } i=5 \text{ (apex)} \end{cases}, \tag{20}$$

$$\begin{aligned}
 dA &= \left(\frac{\partial y}{\partial m} \frac{\partial z}{\partial n} - \frac{\partial y}{\partial n} \frac{\partial z}{\partial m} \right) dm dn \hat{i} - \left(\frac{\partial x}{\partial n} \frac{\partial z}{\partial m} - \frac{\partial x}{\partial m} \frac{\partial z}{\partial n} \right) dm dn \hat{j} + \\
 &\quad \left(\frac{\partial x}{\partial m} \frac{\partial y}{\partial n} - \frac{\partial x}{\partial n} \frac{\partial y}{\partial m} \right) dm dn \hat{k},
 \end{aligned} \tag{21}$$

\rightarrow is this an
index/superscript
 dA
 $d = ?$

where m and n in Eq. (21) represent the local system s, t, or p. The computation of the integration surface area for the remaining element types is similar. Equations (17) - (20) and Eq. (21) are used to evaluate, respectively, the accumulation term (Acc) and the advective flux (F).

$$Acc_{m,i} = \frac{V_{scv_{mj}}}{V_{b,m}} \left(\left(\frac{N_s}{\Delta t} \right)_i^{n+1} - \left(\frac{N_s}{\Delta t} \right)_i^n \right) ; \quad m=1, N_v; i=1, \dots, n_e + 1 \quad (22)$$

$$F_{m,i} = \int_A \sum_{j=1}^{n_p} \left(\xi_j x_j \lambda_j k \left(\frac{\partial \Phi_j}{\partial x_i} \right) \right) dA \quad ?$$

$$\sum_{ip=1}^3 \left(\sum_{j=1}^{n_p} \xi_j x_j \lambda_j k \left. \frac{\partial \Phi_j}{\partial x_i} \right|_{ip} A_n \right); \quad m=1, N_v; n, l=1, \dots, 3; i=1, n_e + 1. \quad (23)$$

From Eq. (23), it is possible to infer that it is necessary calculate molar densities, molar fractions, and molar mobilities at each one of the interfaces of each sub-control volume. Also, it is important to notice that the aforementioned properties are evaluated at the previous time step (superscript n); the superscript 'n+1' denotes the current time-step. In order to evaluate the mentioned properties, an upwind scheme is used. Considering the integration point 1 of Fig. 1, for all the elements, the mobility is calculated as

$$\lambda_{j_{p1}} = \lambda_{j_2} \quad if \quad \left. k \cdot \nabla \Phi_j \cdot dA \right|_{ip1} \leq 0$$

$$\lambda_{j_{p1}} = \lambda_{j_1} \quad if \quad \left. k \cdot \nabla \Phi_j \cdot dA \right|_{ip1} > 0. \quad (24)$$

Inserting Eqs. (22) and (23) in Eq. (8), the final equation for each sub-control volume is given by

$$Acc_{m,i} + F_{m,i} + q_i = 0 ; \quad m=1, \dots, N_v; i=1, \dots, n_e + 1. \quad (25)$$

Eq. (25) represents the material balance for each sub-control volume. The equations for each control-volume are assembled from the contribution of all sub-control volumes that share the same vertex. Further details about this procedure can be found in Marcondes and

12

1
2
3 Sepehrnoori (2010) and Marcondes et al. (2013). A similar procedure realized to the molar
4 balance equation needs to be performed for the pressure equation.
5
6
7
8
9

10 4. RESULTS AND DISCUSSION

11
12 In this section, results for four case studies are presented. The two first case studies are
13 designed to validate the current implementation with the Cartesian implementation of the
14 UTCOMP simulator, and the other two case studies are designed to demonstrate the ability of
15 the EbFVM approach to handle irregular geometries. It is important to emphasize that
16 Cartesian implementation of UTCOMP simulator has been validated using many analytical
17 solutions as well as several commercial simulators. The first case is a CO₂ injection
18 characterized by three hydrocarbon components in a quarter-of-five-spot configuration. The
19 reservoir data, components and composition data, and binary coefficients are shown in Tables
20 1 through 3, respectively.

21 Table 1

22 Table 2

23 Table 3

24
25 The volumetric rates of oil and gas obtained with all the four elements investigated and
26 the refined Cartesian grid are presented in Fig. 2. From this figure, it is possible to infer that
27 all four elements produce results that are in good agreement with the ones obtained with the
28 refined Cartesian grid. Also, the number of volumes for all elements used is much smaller
29 than the ones used by the Cartesian grid, demonstrating that at least for this case study the
30 EbFVM approach is much more accurate than the Cartesian grid. Accuracy can be explained
31 based on the larger Jacobian stencil of the unstructured grid compared to the conventional
32 seven bandwidth diagonals of the Cartesian grid.

33 Figure 2

In order to visualize the pyramid mesh, Figure 3 shows a x-y cut plane through the apex of one pyramid element.

Figure 3

Figure 4 presents the saturation gas field at 500 days for all elements tested and for the Cartesian grid. From this figure, once again it is possible to conclude that very good sharp front were obtained with all elements and these results are in good agreement with the refined Cartesian mesh.

Figure 4

The second case study again refers to a CO₂ injection problem in a quarter-of-five spot and it is characterized with same fluid of case study 1. The difference is that the binary interaction coefficients are all set to zero, which in turn makes the injected fluid completely miscible with the oil in-place.

Figure 5 shows the comparison between the Cartesian grid and the four element types, for case 2, in terms of oil and gas production rates. The results presented in Fig. 5 show a satisfactory match for all elements and the Cartesian grid.

Figure 5

The CO₂ overall mole fraction field at 500 days is shown in Fig. 6. From the results presented, it is possible to observe a good agreement between the EbFVM for all elements and the Cartesian grid.

Figure 6

The third case study again refers to a gas flooding problem in an irregular reservoir characterized by seven hydrocarbon components. The 3D irregular reservoir is shown in Fig. 7. Just to have an idea of the reservoir dimensions, the sizes in Fig. 7 are shown in feet. Two grid configurations are presented in Fig. 7; Fig. 7a shows a grid composed of only

1
2 hexahedron elements, and Fig. 7b shows a hybrid mesh composed of hexahedron,
3 tetrahedron, and pyramids elements.
4
5

6
7 Figure 7
89
10 The reservoir and fluid composition data are given in Tables 4 and 5, respectively.
11
1213 Table 4
14
1516 Table 5
17
1819 Figure 8 shows the oil and gas rates obtained in conjunction with the hexahedron and
20 hybrid (hexahedron, tetrahedron and prism elements) refined grids. From this figure, it is
21 possible to see a good agreement between the results obtained with the two different grid
22 configurations.
23
2425 Figure 8
2627 Figure 9 presents the gas saturation field at two simulated times (100 days; 280 days)
28 obtained with the hexahedron and hybrid grids shown in Figure 7. Although, the grid
29 configurations are completely different from each other, the gas saturation fields presented in
30 Fig. 9 are in good agreement. Also, good resolution fronts with small numerical dispersion
31 were observed.
32
3334 Figure 9
3536 The fourth case study is a mixed fluid (liquid and gas) injection characterized by five
37 hydrocarbon components in a 3D irregular grid. Figure 10 presents two grid configurations: a
38 hexagonal and a hybrid grid. Just to have an idea of the reservoir dimensions, the sizes in Fig.
39 10 are shown in feet. In terms of geometric model, this case is different from case 3, since
40 there is an internal hole that mimics an area of small permeability tensor. If a Cartesian mesh
41 is used to model such an area, inactive cells should be used. Using the EbFVM approach, no
42 additional calculation is necessary.
43
4445 Figure 10
46
47

1
2
3 The reservoir and fluid composition information are shown in Tables 6 and Table 7,
4
5 respectively.
6

7
8 Table 6
9
1011 Table 7
12
13
14
15
16
17

Figure 11 presents the oil and gas rates in conjunction with the hexahedron and hybrid grids. From this figure, is possible to observe a very good match between the two grid configurations investigated.

18 Figure 11
19
20
21
22
23

The gas saturation fields at 200 and 1000 days are presented in Figure 12. Once again, an excellent gas saturation front with both grid configurations is observed.

24 Figure 12
25
26
27
28
29
30
31
32

In order to visualize the hybrid grid, it is shown in Fig. 13 a cut plane passing through an injection well and a production well. From this figure, it is possible to see the gas saturation profile, as well as the hybrid grid around the wells.

33 Figure 13
34
35
36
37
38
39

5. CONCLUSIONS

40
41
42 This work presented the implementation of an EbFVM formulation using unstructured
43 grids for tridimensional compositional reservoir simulation in conjunction with an IMPEC
44 approach. The method was applied using four element types: hexahedron, tetrahedron, prism,
45 and pyramid. Four different case studies are presented in order to validate and show the
46 flexibility and the accuracy of the EbFVM approach compared to the commonly used
47 Cartesian grids. From the results obtained, it is possible to observe that EbFVM can be an
48
49
50
51
52
53
54
55
56
57
58
59
60

1
2 excellent methodology to handle important geometric parameters of the reservoirs with a high
3 level of accuracy.



NOMENCLATURE

A	Area (m^2)
Acc	Accumulation term of the material balance (mol/d)
c_f	Rock compressibility (Pa^{-1})
F	Advection flux term of the material balance (mol/d)
f	Fractionary flow or fugacity for the equilibrium constraint
g	Gravity (m/d^2)
J	Mole flux transported by dispersion (mol/ $\text{m}^2 \text{ d}$)
K	Equilibrium ratio
\bar{K}	Absolute permeability tensor (m^2)
k_r	Relative permeability
N	Number of moles (mol) or shape function
n_c	Number of components
n_p	Number of phases
P	Pressure (Pa)
q	Well mole rate (mol/d)
S	Saturation
t	Time (s)
V_b	Bulk volume (m^3)
V_p	Pore volume (m^3)

1	V_t	Total fluid volume (m^3)
2	\bar{V}_i	Total fluid Partial molar volume (m^3/mol)
3	\bar{V}_g	Phase partial molar volume (m^3/mol)
4	x	Phase mole fraction
5	z	Overall mole fraction

Greek Letters

21	ξ	Mole density (mol/m^3)
22	ϕ	Porosity
23	λ	Phase mobility ($\text{Pa}^{-1} \text{ d}^{-1}$)
24	Φ	Hydraulic potential (Pa)
25	μ	Viscosity (Pa d)
26	ν	Molar fraction in the absence of water

Superscripts

41	n	Previous time step level
42	$n+1$	New time step level

Subscripts

51	i	Control volume
52	j	Phase
53	k	Component

1
2 r Reference phase
3
4 t Total
5
6
7
8
9

ACKNOWLEDGMENTS

10
11
12
13 The authors would like to acknowledge PETROBRAS S/A Company for the financial
14 support for this work. Also, the authors would like to thank ESSS Company for providing
15 Kraken® to pre and post-processing the results. Finally, Francisco Marcondes would like to
16 acknowledge CNPq (The National Council for Scientific and Technological Development of
17 Brazil) for its financial support through grant No. 305415/2012-3.
18
19
20
21
22
23
24
25
26
27
28
29
30
31
32
33
34
35
36
37
38
39
40
41
42
43
44
45
46
47
48
49
50
51
52
53
54
55
56
57
58
59
60

5. REFERENCES

- Ács, G., Doleschall, S. and Farkas, E., General Purpose Compositional Model. SPE Journal, 25, p. 543-553 (1985).
- Baliga B.R. and Patankar SV, A Control Volume Finite-Element Method for Two-Dimensional Fluid Flow and Heat Transfer. Numerical Heat Transfer, 6(3), p.245-261 (1983).
- Chang, Y.-B., Development and Application of an Equation of State Compositional Simulator. Phd Thesis. The University of Texas at Austin (1990).
- Cordazzo J, Maliska CR, Silva AFC, Hurtado FSV, The Negative Transmissibility Issue When Using CVFEM in Petroleum Reservoir Simulation - 1. Theory. The 10th Brazilian Congress of Thermal Sciences and Engineering, Rio de Janeiro, Brazil, 29 Nov – 03 Dec (2004).
- Cordazzo J, Maliska CR, Silva AFC, Hurtado FSV, The Negative Transmissibility Issue When Using CVFEM in Petroleum Reservoir Simulation - 2. Results. The 10th Brazilian

1
2 Congress of Thermal Sciences and Engineering, Rio de Janeiro, Brazil, 29 Nov – 03 Dec
3 (2004).
4
5

6 Cordazzo J, An Element Based Conservative Scheme using Unstructured Grids for Reservoir
7 Simulation. The SPE Annual Technical Conference and Exhibition, Houston, USA, 26-29
8 Sept (2004).
9
10

11 Edwards MG, Unstructured, Control-volume Distributed, Full-Tensor Finite-Volume
12 Schemes with Flow Based Grids. Computational Geosciences, 6(3-4) p. 433-452 (2002).
13
14

15 Fernandes BRB, Marcondes F, Sepehrnoori K, Investigation of Several Interpolation
16 Functions for Unstructured Meshes in Conjunction with Compositional Reservoir Simulation.
17 Numerical Heat Transfer part A: Applications, 64(12), p. 974-993 (2013).
18
19

20 Forsyth PA, A Control-Volume, Finite-Element Method for Local Mesh Refinement in
21 Thermal Reservoir Simulation. SPE Reservoir Engineering 1990, 5(4), p. 561-566 (1990).
22
23

24 Fung LS, Hiebert AD, Nghiem L, Reservoir Simulation with a Control-Volume Finite-
25 Element Method. The 11th SPE Symposium on Reservoir Simulation, Anaheim, USA, 17-20
26 Feb (1991).
27
28

29 Gottardi G, Dall'Olio D, A Control-Volume Finite-Element Model for Simulating Oil-Water
30 Reservoirs. Journal of Petroleum Science and Engineering, 8(1), p. 29-41 (1992).
31
32

33 Hughes TJR, The Finite Element Method, Linear Static and Dynamic Finite Element
34 Analysis. New Jersey, Prentice Hall (1987).
35
36

37 Marcondes F, Santos LOS, Varavei A, Sepehrnoori K, A 3D Hybrid Element-based Finite-
38 volume Method for Heterogeneous and Anisotropic Compositional Reservoir Simulation.
39 Journal of Petroleum Science & Engineering, 108, p. 342-351 (2013).
40
41

42 Marcondes F, Sepehrnoori K, An Element-Based Finite-Volume Method Approach for
43 Heterogeneous and Anisotropic Compositional Reservoir Simulation. Journal of Petroleum
44 Science & Engineering, 73(1-2), p. 99-106 (2010).
45
46
47
48
49
50
51
52
53
54
55
56
57
58
59
60

20

- 1
2 Paluszny A, Matthäi SK, Hohmeyer M, Hybrid Finite Element-Finite Volume Discretization
3 of Complex Geologic Structures and a New Simulation Workflow Demonstrated on
4 Fractured Rocks. *Geofluids*, 7(2), p. 186-208 (2007).
- 5
6 Raw M, A New Control Volume Based Finite Element Procedure for the Numerical Solution
7 of the Fluid Flow and Scalar Transport Equations. PhD Thesis. University of Waterloo
8 (1985).
- 9
10 Santos LOS, Marcondes F, Sepehrnoori K. A 3D compositional miscible gas flooding
11 simulator with dispersion using Element-based Finite-Volume method. *Journal of Petroleum*
12 Science & Engineering, 112, p. 61-68 (2013).
- 13
14 Verma S, Aziz K, A Control Volume Scheme for Flexible Grids in Reservoir Simulation. The
15 Reservoir Simulation Symposium, Dallas, USA, 8-11 Jun (1997).
- 16
17 Wang P, Yotov I, Wheeler M, Arbogast T, Dawson C, Parashar M, Sepehrnoori K. A New
18 Generation EOS Compositional Reservoir Simulator: Part I – Formulation and Discretization.
19 SPE Reservoir Simulation Symposium, Dallas, USA, 8-11 Jun (1997).

Figure Captions

Figure 1. Sub-control volumes for the four element types: (a) hexahedron, (b) tetrahedron, (c) prism, and (d) pyramid

Figure 2. Volumetric rates - Case 1: a) Oil and b) Gas

Figure 3. Aerial view of the cut plane of the pyramid mesh

Figure 4. Gas saturation at 500 days for Case 1. (a) Cartesian; (b) Hexahedron; (c) Prism; (d) Tetrahedron and (e) Pyramid

Figure 5. Volumetric rates - Case 2: a) Oil and b) Gas

Figure 6. CO₂ overall mole fraction fields for Case 2 at 500 days. (a) Cartesian; (b) Hexahedron; (c) Prism; (d) Tetrahedron and (e) Pyramid

Figure 7. Grid configurations used for Case 3. (a) Hexahedron grid (14896 vertices; 12987 elements) and (b) hybrid grid (19928 vertices; 14352 tetrahedrons; 12688 hexahedrons; 7800 pyramids)

Figure 8. Volumetric rates for Case 3. a) Oil and b) Gas

Figure 9. Gas saturation fields for Case 3. Hexahedron: a) 100 days, b) 280 days. Hybrid: c) 100 days, d) 280 days

Figure 10. Grid configurations used for Case 4. (a) Hexahedron grid (41392 vertices; 36975 elements) and (b) hybrid grid (42232 vertices; 4200 tetrahedrons; 35715 hexahedrons; 4200 pyramids)

Figure 11. Volumetric rates for Case 4. a) Oil and b) Gas

Figure 12. Gas saturation fields for Case 4. Hexahedron: a) 200 days, b) 1000 days. Hybrid: c) 200 days, d) 1000 days

Figure 13. Cut plane through wells - gas saturation in 1000 days

Table Captions

Table 1 Reservoir data for Case 1

Table 2 Fluid composition data for Case 1

Table 3 Binary interaction coefficients for Case 1

Table 4 Reservoir data for Case 3

Table 5 Fluid composition data for Case 3

Table 6 Reservoir data for Case 4

Table 7 Fluid composition data for Case 4

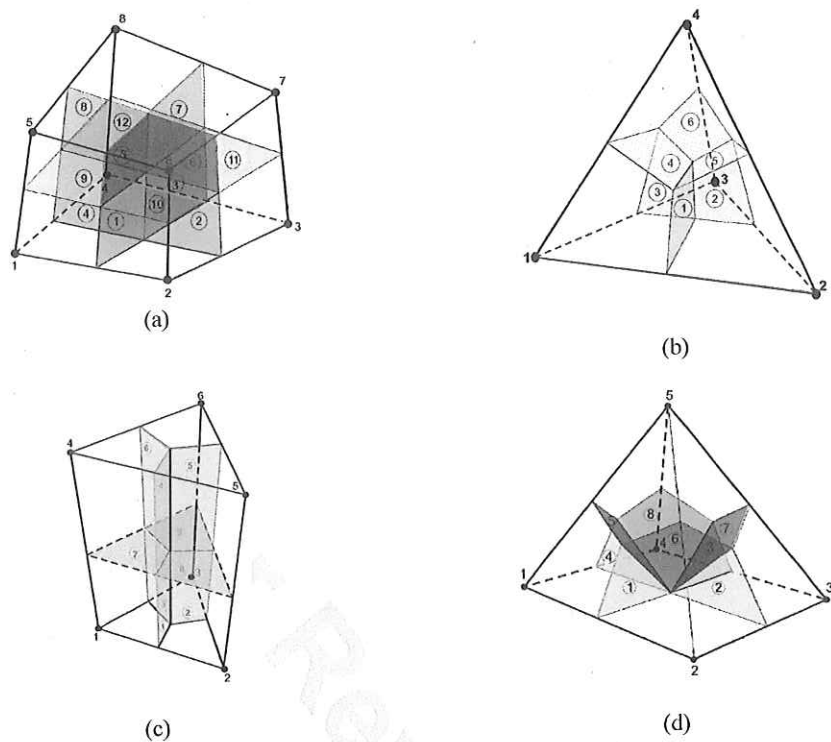


Figure 1. Sub-control volumes for the four element types: (a) hexahedron, (b) tetrahedron, (c) prism, and (d) pyramid

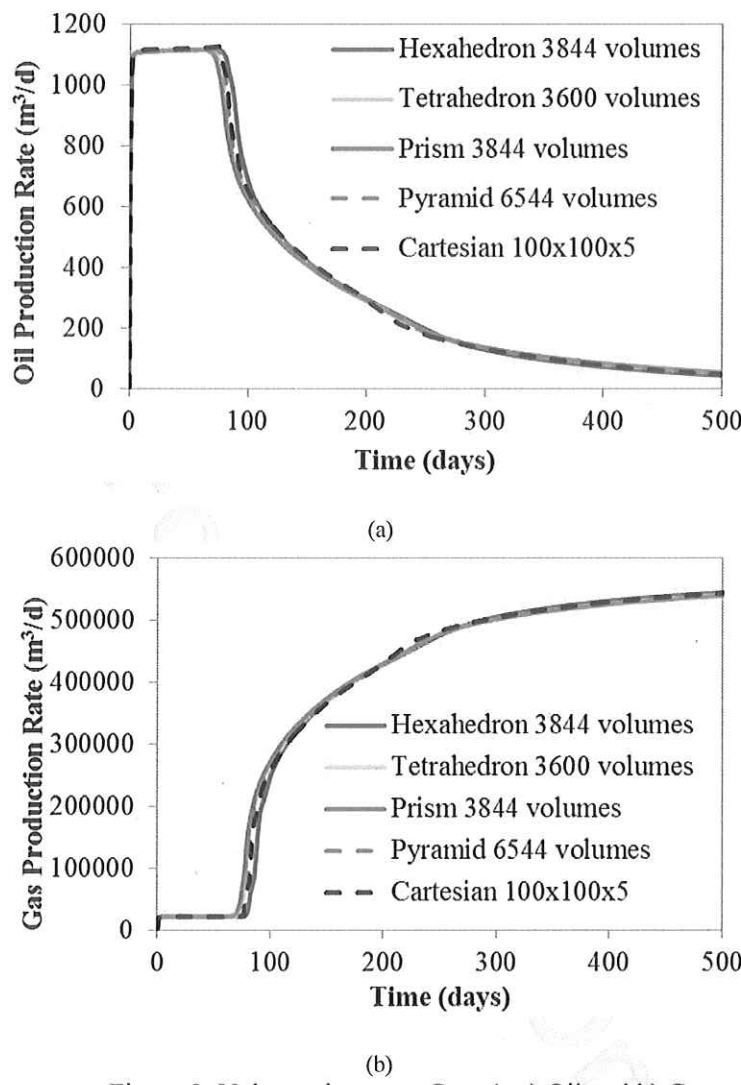


Figure 2. Volumetric rates - Case 1: a) Oil and b) Gas

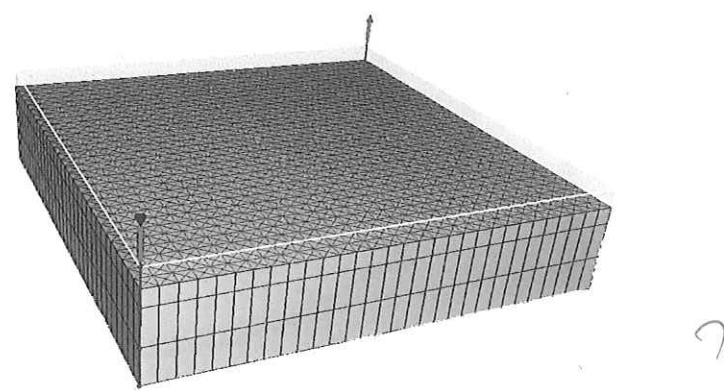


Figure 3. Aerial view of the cut plane of the pyramid mesh

1
2
3
4
5
6
7
8
9
10
11
12
13
14
15
16
17
18
19
20
21
22
23
24
25
26
27
28
29
30
31
32
33
34
35
36
37
38
39
40
41
42
43
44
45
46
47
48
49
50
51
52
53
54
55
56
57
58
59
60

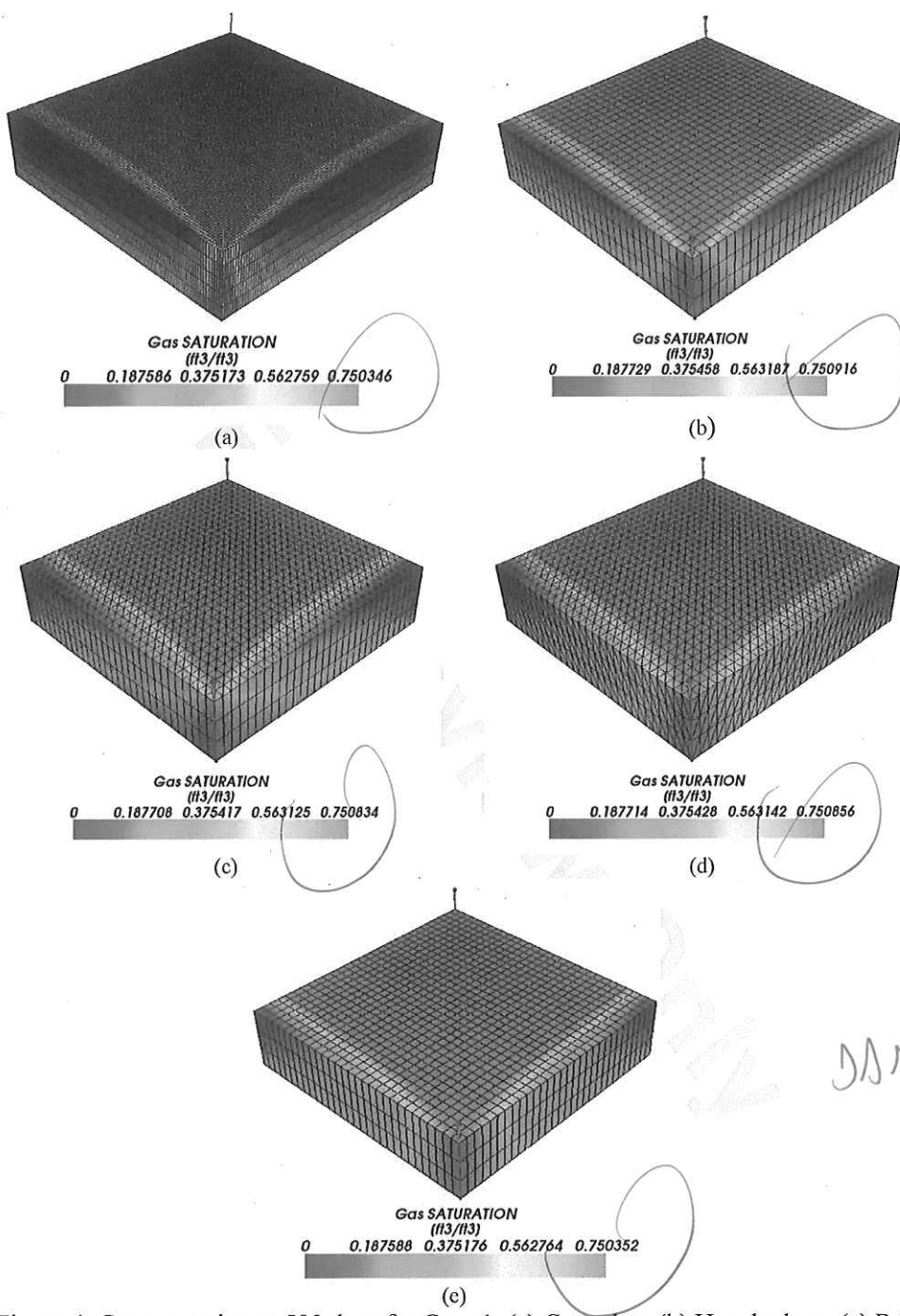


Figure 4. Gas saturation at 500 days for Case 1. (a) Cartesian; (b) Hexahedron; (c) Prism; (d) Tetrahedron and (e) Pyramid

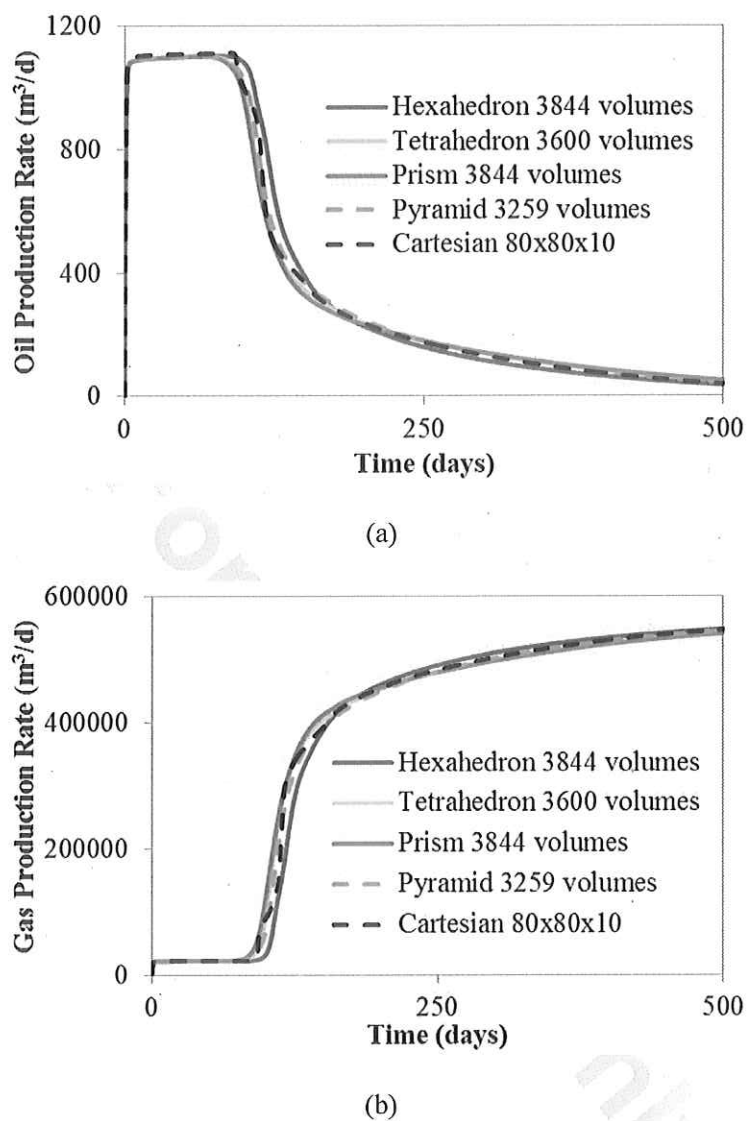


Figure 5. Volumetric rates - Case 2: a) Oil and b) Gas

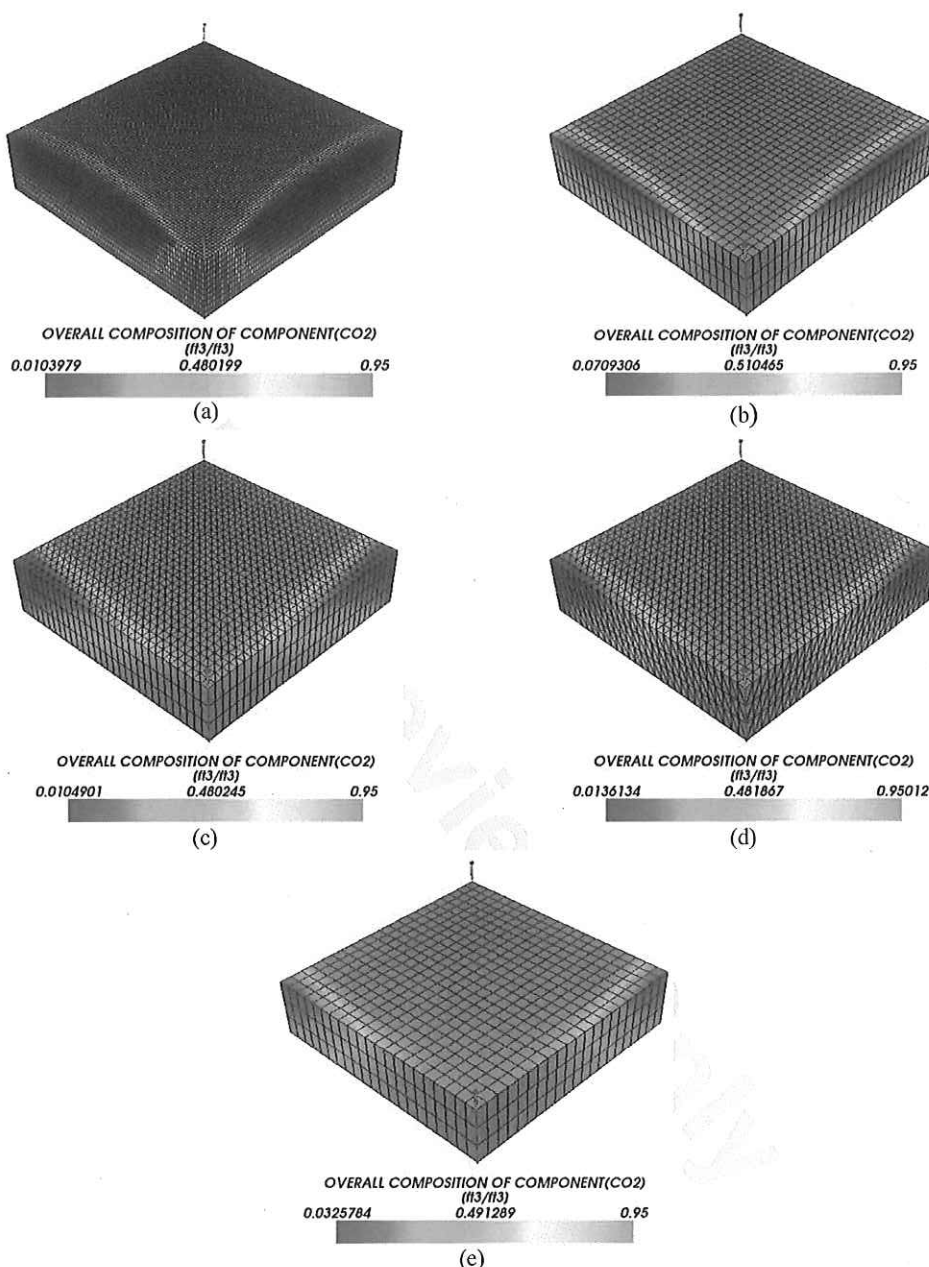


Figure 6. CO₂ overall mole fraction fields for Case 2 at 500 days. (a) Cartesian; (b) Hexahedron; (c) Prism; (d) Tetrahedron and (e) Pyramid

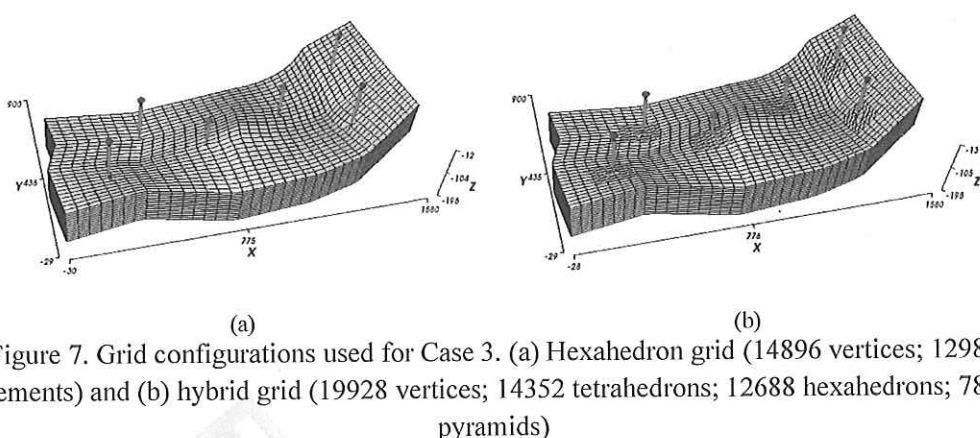


Figure 7. Grid configurations used for Case 3. (a) Hexahedron grid (14896 vertices; 12987 elements) and (b) hybrid grid (19928 vertices; 14352 tetrahedrons; 12688 hexahedrons; 7800 pyramids)

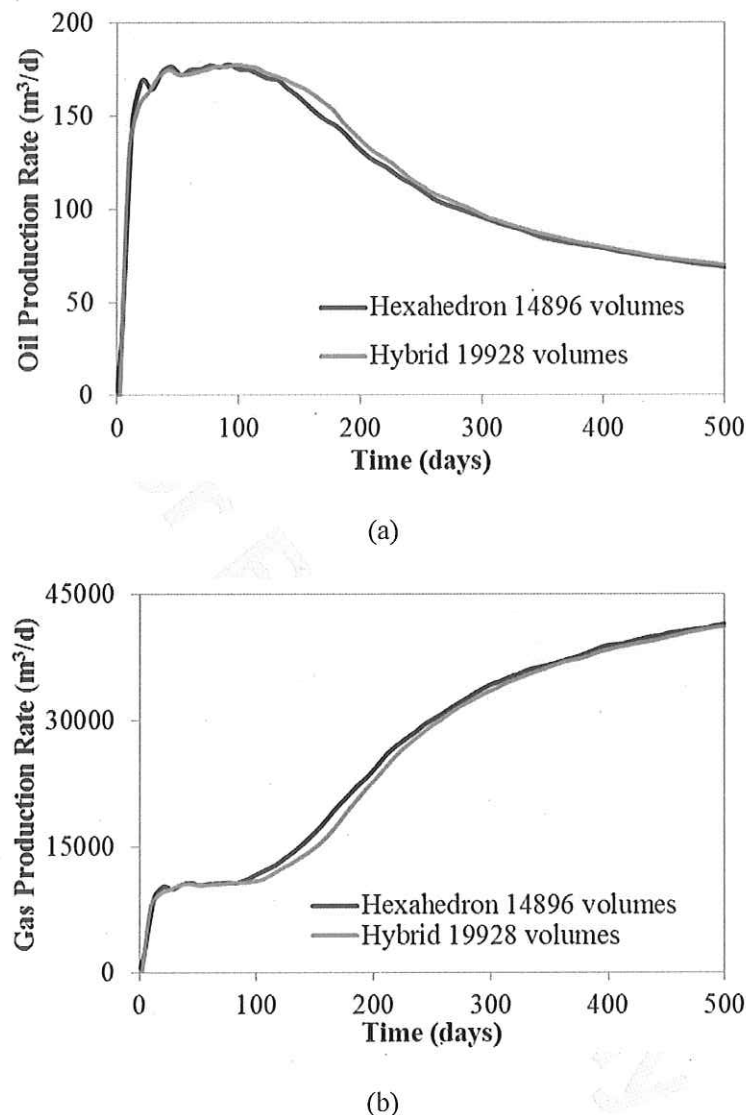


Figure 8. Volumetric rates for Case 3. a) Oil and b) Gas

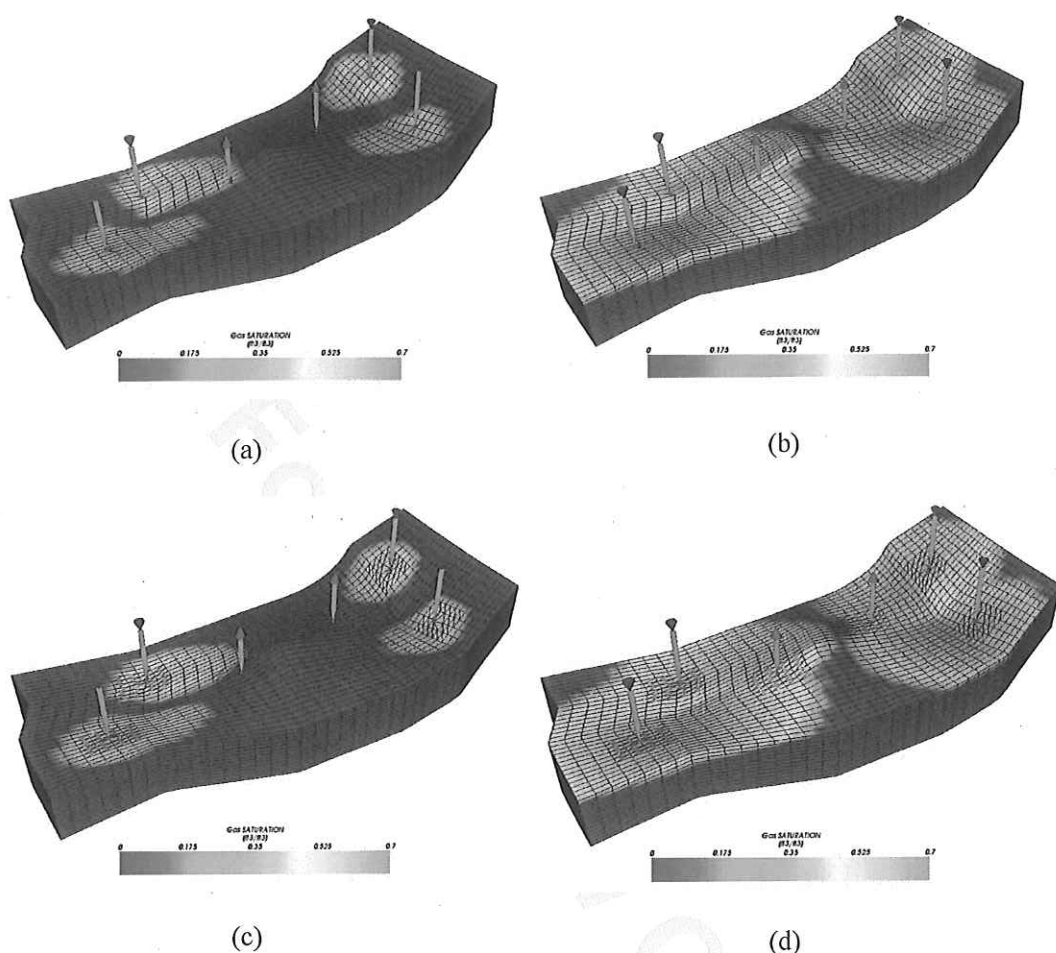


Figure 9. Gas saturation fields for Case 3. Hexahedron: a) 100 days, b) 280 days. Hybrid: c) 100 days, d) 280 days

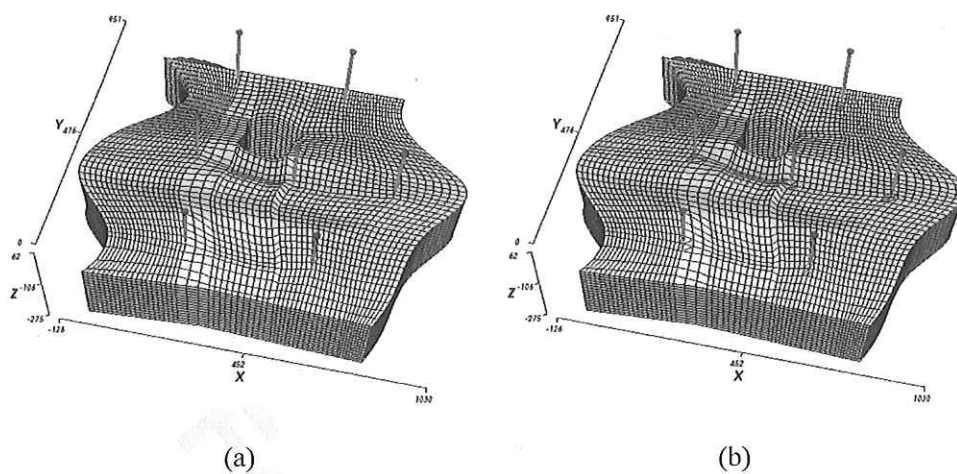
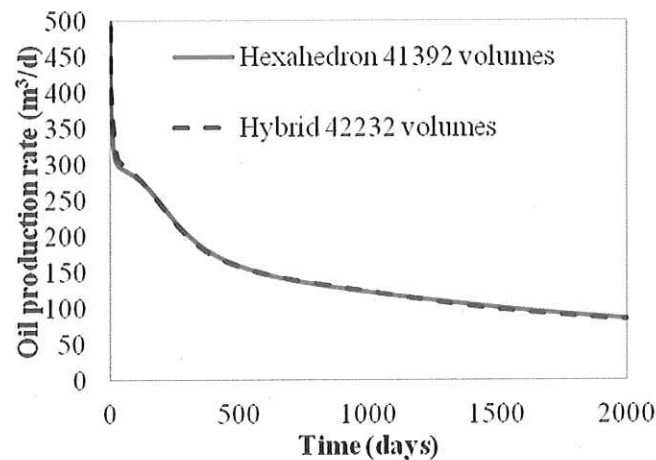
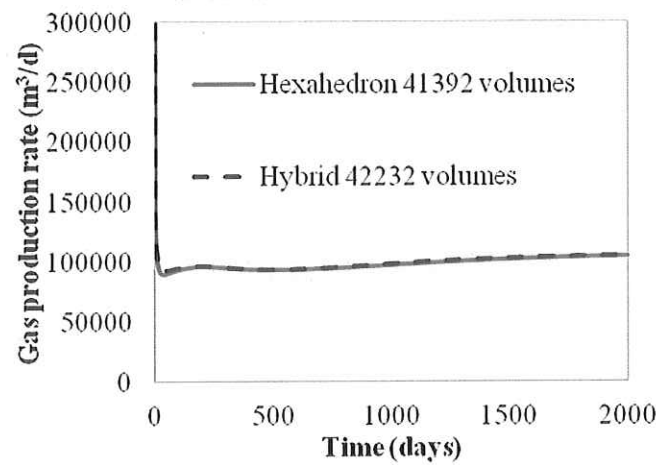


Figure 10. Grid configurations used for Case 4. (a) Hexahedron grid (41392 vertices; 36975 elements) and (b) hybrid grid (42232 vertices; 4200 tetrahedrons; 35715 hexahedrons; 4200 pyramids)



(a)



(b)

Figure 11. Volumetric rates for Case 4. a) Oil and b) Gas

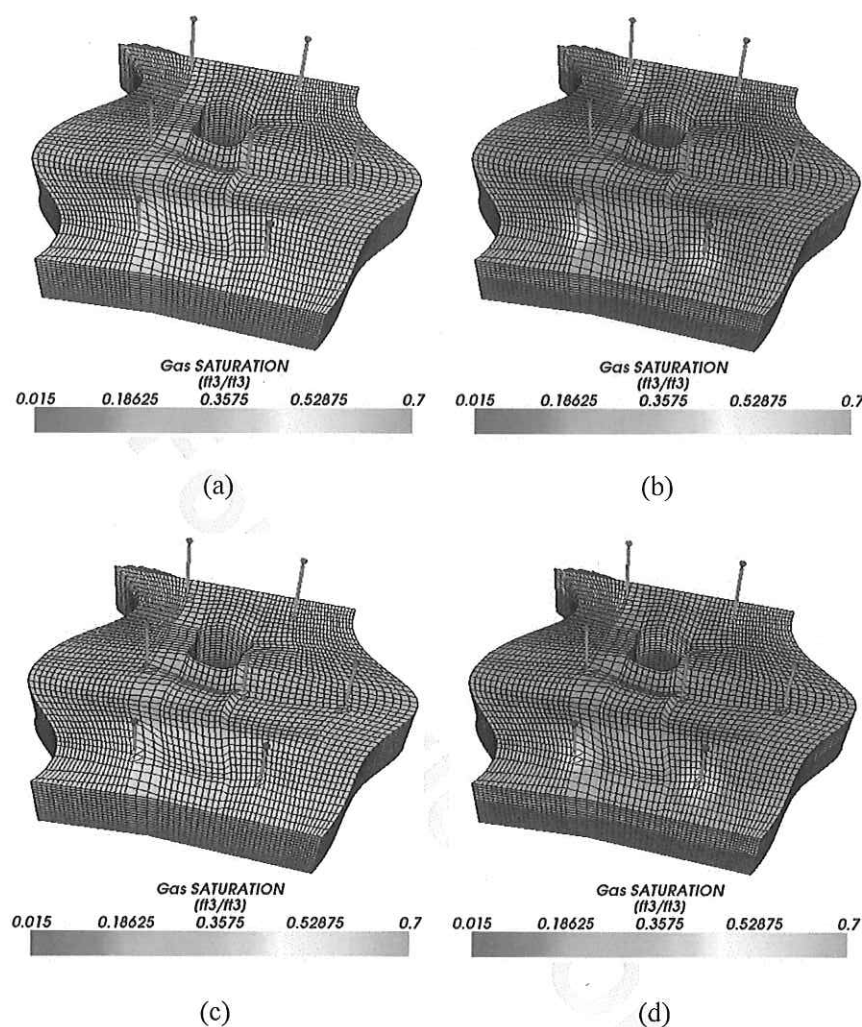


Figure 12. Gas saturation fields for Case 4. Hexahedron: a) 200 days, b) 1000 days. Hybrid:
c) 200 days, d) 1000 days

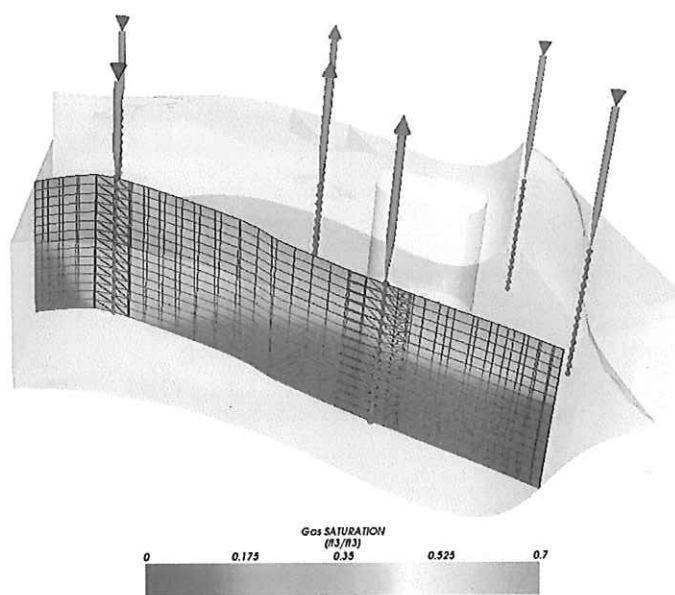


Figure 13. Cut plane through wells - gas saturation in 1000 days

Table 1. Reservoir data for Case 1.

Property	Value
Length, width, and thickness	170.69 m, 170.69 m, and 30.48 m
Porosity	0.30
Initial Water Saturation	0.25
Initial Pressure	20.65 MPa
Permeability in X, Y, and Z directions	1.974×10^{-13} m ² , 1.974×10^{-13} m ² , and 1.974×10^{-14} m ²
Formation Temperature	299.82 K
Gas Injection Rate	5.66×10^2 m ³ /d
Producer's Bottom Hole Pressure	20.65 MPa

Table 2. Fluid composition data for Case 1.

Component	Initial Reservoir Composition	Injection Fluid Composition
CO ₂	0.0100	0.9500
C ₁	0.1900	0.0500
n-C ₁₆	0.8000	-

Table 3. Binary interaction coefficients for Case 1.

Component	CO ₂	C ₁	n-C ₁₆
CO ₂	-	0.12	0.12
C ₁	0.12	-	-
n-C ₁₆	0.12	-	-

Table 4. Reservoir data for Case 3.

Property	Value
Porosity	0.163
Initial Water Saturation	0.25
Initial Pressure	19.65 MPa
Permeability in X, Y, and Z directions	$1.974 \times 10^{-13} \text{ m}^2$, $1.974 \times 10^{-13} \text{ m}^2$, and $1.974 \times 10^{-14} \text{ m}^2$
Formation Temperature	400 K
Gas Injection Rate	$14.16 \times 10^3 \text{ m}^3/\text{d}$
Producer's Bottom Hole Pressure	19.65 MPa

Table 5. Fluid composition data for Case 3.

Component	Initial Reservoir Composition	Injection Fluid Composition

40

1	CO ₂	0.0077	0.96
2	C ₁	0.2025	0.01
3	C ₂ -C ₃	0.1180	0.01
4	C ₄ -C ₆	0.1484	0.01
5	C ₇ -C ₁₄	0.2863	0.01
6	C ₁₅ -C ₂₄	0.1490	-
7	C ₂₅₊	0.0881	-

Table 6. Reservoir data for Case 4.

Property	Value

1	Porosity	0.35
2	Initial Water Saturation	0.17
3	Initial Pressure	10.34 MPa
4	Permeability in all directions	$9.869 \times 10^{-15} \text{ m}^2$
5	Formation Temperature	344.26 K
6	Gas Injection Rate	$28.32 \times 10^3 \text{ m}^3/\text{d}$
7	Producer's Bottom Hole Pressure	8.96 MPa

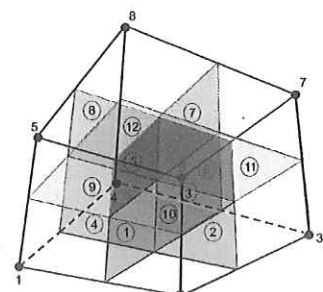
Table 7. Fluid composition data for Case 4.

Component	Initial Reservoir Composition	Injection Fluid Composition

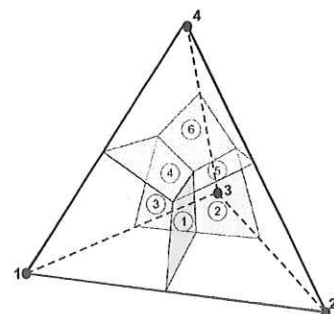
42

	C ₁	0.5000	0.7700
	C ₃	0.0300	0.2000
	C ₆	0.0700	0.0100
	C ₁₀	0.2000	0.0100
	C ₁₅	0.1500	0.0050
	C ₂₀	0.0500	0.0050

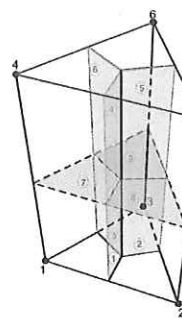
1
2
3
4
5
6
7
8
9
10
11
12
13
14
15
16



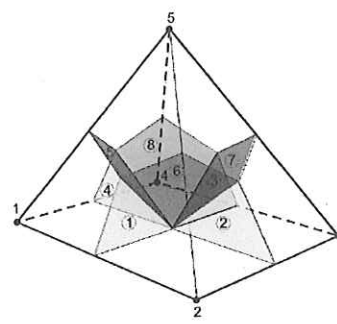
(a)



(b)



(c)



(d)

Fig. 1.

17
18
19
20
21
22
23
24
25
26
27
28
29
30
31
32
33
34
35
36
37
38
39
40
41
42
43
44
45
46
47
48
49
50
51
52
53
54
55
56
57
58
59
60